International Journal of Smart Control and Electrical Engineering Systems (IJSCEES)
Vol. 1, No. 2, December 2026, pp. 89-108
ISSN: 3137-168X

Design and Analysis of a Single-Fed Circularly Polarized MPA at 2.4GHz Using Symmetrical Slits for WLAN and ISM-Band Applications

Idris Saadu Idris [1], S. H. Lawan [2], Nasir Farouk [3], A. H. Jabire [4], Munzali Ahmed Abana [5]
[1] Department of Electrical Engineering, Pan African University Institute for Basic Sciences, Technology and Innovation (PAUSTI), Nairobi, Kenya
[2] Department of Electrical Engineering, Bayero University, Kano, Nigeria
[3] Department of Information Technology. Sule Lamido University, Kafin Hausa, Nigeria.
[4] Department of Electric Engineering, Taraba State University, Jalingo, Nigeria.
[5] Department of Electric Engineering, Modibbo Adama University, Yola, Nigeria.

Article Information

Article History:

Received 25 June 2026
Revised 06 September 2026
Accepted 07 September 2026

Keywords:

LHC Polarization;
RHC Polarization;
Linear Polarization;
WLAN;
ISM-Band.

Corresponding Author:

Idris Saadu Idris,
Bayero University, Kano,
Kano, Nigeria.
Isi1800062.mee@buk.edu.ng

This work is open access under a Creative Commons Attribution-Share Alike 4.0

Abstract

This paper presents the design and numerical evaluation of a compact, single-fed, circularly polarized (CP) microstrip patch antenna operating at 2.4 GHz. It is intended for use in wireless communication systems that operate within the WLAN and ISM frequency bands. The antenna features a circular radiating patch with symmetrically placed slits used to excite two orthogonal modes with equal amplitude and a 90-degree phase difference. This setup enables circular polarization generation from a single feed point. The antenna is constructed on an FR4 substrate with a relative permittivity of 4.3 and a thickness of 1.6 mm. This material choice makes the antenna easy to manufacture using standard printed circuit board (PCB) techniques. The design overcomes the shortcomings of traditional linearly polarized antennas, which are often affected by polarization mismatch and performance issues in environments with multiple signal paths. By achieving circular polarization through a straightforward geometric change rather than complex feeding structures, the antenna remains structurally simple while improving radiation performance when the orientation of the transmitting and receiving antennas may vary. The antenna's performance was analyzed using full-wave electromagnetic simulations conducted in CST Microwave Studio. The simulation results show that the antenna provides consistent circular polarization, is compact, and is well-suited for use in modern, low-profile wireless devices.

Citation Document:

I. S. Idris, S. H. Lawan, N. Farouk, A. H. Jabire, and M. A. Abana, "Design and analysis of a single-fed circularly polarized MPA at 2.4 GHz using symmetrical slits for WLAN and ISM-band applications," International Journal of Smart Control and Electrical Engineering Systems (IJSCEES), vol. 1, no. 2, pp. 89–108, Dec. 2026.

1. Introduction

Circular polarisation (CP) antennas have become more popular in recent years. This is mainly because they handle issues like multipath distortion and polarisation mismatch better than linear polarisation [1]. With circular polarisation, the antennas used for sending and receiving don't have to be perfectly aligned [1], [2]. Also, CP antennas are popular in satellite and mobile communication systems because they are cheap, small, and easy to integrate [2]. In modern wireless communication systems, antennas play a vital role. These components must meet higher performance demands to improve wireless issues [2], especially to facilitate their integration into small devices such as 5G systems [3]. The need for low-cost, compact, and miniature antennas has received considerable attention in recent developments [3]. Recently, advancements have been made in miniaturized antenna configurations using various methods to meet practical applications. These advancements have been observed in slotted patch antennas [3], multilayer antenna structures [4], array

antennas [5], and other SIW-based antenna models [5]. However, miniaturization often degrades performance, such as reducing gain or bandwidth, revealing limitations of these methods, some of which may be complicated to manufacture.

Numerous research efforts [2-5] have effectively created antennas exhibiting circular polarization. Nevertheless, circularly polarized antennas face the drawback of greater cross-polarization interference, leading to decreased signal transmission efficiency and heightened vulnerability to interference in satellite communication systems. Circular polarization must be thoughtfully evaluated based on application needs and environmental operating conditions. Research has examined antennas designed for communication using single linear polarization, as shown in [5]. Single linear polarization has drawbacks, including increased interference, limited capacity, and reduced signal quality in multipath conditions. Cross-polarization antennas for transmission and reception are essential to improve the effectiveness and reliability of satellite communication systems in high-interference environments with substantial data capacity requirements. These systems need antennas with dual linear polarization to integrate with existing infrastructure and meet operational requirements. Dual linear polarization antennas enable concurrent transmission and reception on two orthogonal polarizations, effectively increasing communication capacity and improving overall system performance. Multiple methods have been established for designing dual-polarized antennas, such as aperture-coupled microstrip antennas [6], two-port feed networks [6], and the implementation of two or more feed probes [7]. Nonetheless, every method presents its difficulties. Aperture-coupled microstrip antennas necessitate intricate designs, which may present

fabrication difficulties and heightened losses from aperture radiation, with restricted bandwidth as a typical limitation. Meanwhile, two-port power feed networks provide effective power distribution, but they require more intricate designs, demand extra space, and incur power losses along the transmission routes, potentially reducing efficiency. Using two or more feed probes may increase mutual coupling, which affects performance, polarization isolation, and sensitivity to physical asymmetry, requiring complex impedance matching and complicating the design process. The contributions of this study are as follows:

a) A new slit-loaded circular patch design that achieves circular polarization by exciting two perpendicular modes with a 90-degree phase difference using a single feed.
b) A compact and low-profile antenna structure made using cost-effective FR4 material, suitable for 2.4 GHz WLAN and ISM band applications.
c) Avoidance of complex dual-feed systems or external phase-shifting circuits, which simplifies the manufacturing process and reduces the overall complexity of implementation.
d) A comprehensive full-wave simulation analysis conducted using CST software, demonstrating consistent circular polarization and suitability for modern wireless devices operating in multipath environments.

2. Literature Review / Related Work

This paper presents the design and performance of a circularly polarised microstrip patch antenna for Wireless Local Area Network (WLAN) applications. The antenna is a proximity-coupled microstrip patch antenna with a V-slot loaded on the radiating patch. This miniaturized microstrip antenna possesses a broad bandwidth within the WLAN frequency range and demonstrates circular polarisation in the far field, exhibiting an excellent axial ratio bandwidth. The simulated outcomes generated by the IE3D program are corroborated by empirical measurements [8].

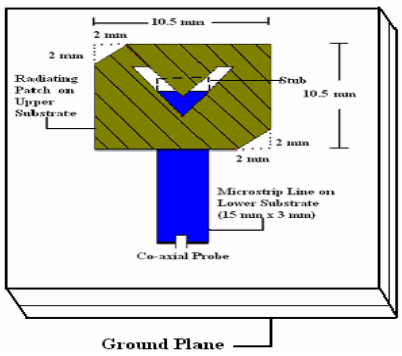

Figure 1. Geometry of the proximity-coupled V-slot-loaded microstrip antenna [8].

This paper presents the design and performance evaluation of a 2.4 GHz helical antenna for effective wireless communication in situations with considerable signal reflections. Helical antennas, known for their ability to deliver circular polarisation and high directivity, are an optimal choice for reducing interference in demanding environments. The antenna is engineered using key parameters such as helix diameter, turn spacing, and pitch angle, and optimized for operation at 2.4 GHz. A comprehensive methodology based on theoretical equations guides the design process, ensuring accurate performance. The assessed antenna demonstrates a minimal return loss of -30.89 dB, a voltage standing wave ratio of 1.05, and elevated directivity and gain values of 8.08 dBi and 8.23 dBi, respectively. The results indicate that the suggested helical antenna satisfies the performance criteria for contemporary wireless communication applications, providing a dependable solution for systems including Wi-Fi, Bluetooth, and IoT networks [9].

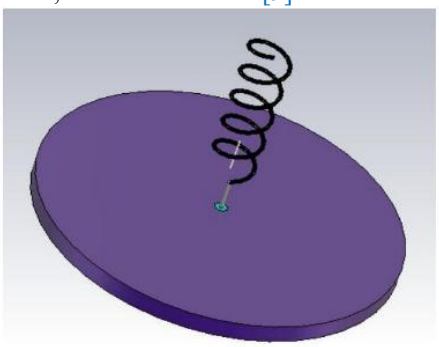

Figure 2: Geometry of the 2.4 GHz helical antenna [9].

3. Antenna Design Methodology

Deschamps first proposed the microstrip antenna in 1953 [8]. It was patented in 1955 [9], but the first antenna was built in the 1970s, when suitable substrates became available. Since then, microstrip antennas have steadily evolved into one of the most appealing antenna choices in various contemporary microwave systems. The rapid expansion of microstrip antenna applications and functions has driven ongoing research to enhance and refine its properties [10-11].

In 1981, Carver and Mink [12] published a study on microstrip antenna technology that outlined analytical methods, design procedures, and the functioning of circular polarization in microstrip components. In 1983, Sharma [13] analyzed how to improve the positioning of a single feed to achieve circularly polarized behavior in microstrip antennas. In 1997, Wong et al. [14] presented a paper that explained the operation of a square patch antenna with circular polarization. In 1998, Huang et al. [15] and Chen et al. [16] both released foundational papers discussing the circular polarization of microstrip antennas. In 2002, Langston et al. [17] developed analytical formulas for the impedance bandwidth, axial ratio, and received power bandwidths of both linearly and circularly polarized microstrip antennas.

This paper introduces the design of a microstrip antenna that achieves circular polarization.

Circular polarization is accomplished by trimming the corners of the patch, creating slits, and strategically placing these slits in the diagonal arms. This design represents a notable improvement over previous studies reviewed in literature. This study will meet the antenna demands of affordability, compactness, high gain, wide operational bandwidth, and favorable radiation patterns, thus addressing the drawbacks of the circular polarization microstrip antenna

3.1. Design specification

The antenna is designed for the lower 2.4 GHz ISM allocation with a nominal design frequency of 2.4 GHz. The substrate is standard FR-4 with a relative permittivity of 4.3 and a thickness of 1.6 mm, selected for cost and for compatibility with conventional PCB etching. The radiator is a circular patch excited by a single coaxial probe, and circular polarization is produced by symmetrically placed slits rather than by a feed network [18-25].

3.2. Circular patch dimensions

The free-space wavelength at design frequency is obtained from the following Equation (1):

$$\lambda_0 = \frac{c}{f_r} \tag{1}$$

where c is the velocity of light in free space and f_r is the resonant frequency. At 2.4 GHz, this gives $\lambda_0 =$ 125.0 mm.

A circular patch supports the dominant TM110 mode, whose resonant frequency is governed by the first zero of the derivatives of the Bessel function of the first kind and first order, $\chi'_{11} = 1.8412$. Neglecting fringing, the resonance condition is as depicts in Equation (2):

$$f_r = \frac{\chi'_{11} c}{2\pi a_e \sqrt{\varepsilon_r}} = \frac{1.8412\, c}{2\pi a_e \sqrt{\varepsilon_r}} \tag{2}$$

Where the a_e is the effective radius of the patch and ε_r is the relative permittivity of the substrate. Because the fringing field at the rim makes the patch appear electrically larger than its physical size, the physical radius must be obtained from an implicit relation. Following the cavity model, an intermediate design parameter is first defined as given by Equation (3):

$$F = \frac{8.791 \times 10^9}{f_r \sqrt{\varepsilon_r}} \tag{3}$$

with f_r in hertz and F in centimetres. The physical radius of the circular patch then follows from the following Equation (4):

$$a = \frac{F}{\sqrt{1 + \frac{2h}{\pi \varepsilon_r F}\left[\ln\left(\frac{\pi F}{2h}\right) + 1.7726\right]}} \tag{4}$$

where h is the substrate thickness, expressed in the same units as F. The corresponding effective radius, which accounts for the fringing field and is the quantity that enters (2), is as present in Equation (5):

$$a_e = a\sqrt{1 + \frac{2h}{\pi \varepsilon_r a}\left[\ln\left(\frac{\pi a}{2h}\right) + 1.7726\right]} \tag{5}$$

Substituting $f_r = 2.4$ GHz, $\varepsilon_r = 4.3$ and $h = 1.6$ mm into (3) gives $F = 17.664$ mm, and (4) then yields a physical radius of $a = 17.14$ mm for an unperturbed circular patch. Introducing the slits lengthens the surface-current path and lowers the resonance, so the radius was reduced during optimization to the final value $a = 16.701$ mm reported in Table 1. Evaluating (5) at this radius gives $a_e = 17.234$ mm and substituting back into (2) returns 2.460 GHz for the corresponding un-slitted patch. The downward shift of approximately 2.5 percent produced by the slit loading therefore brings the loaded structure to the intended 2.4 GHz design point, which confirms the internal consistency of the procedure.

The effective relative permittivity seen by the patch, required for the guided wavelength and for the feed design, is defined by Equation (6):

$$\varepsilon_{reff} = \frac{\varepsilon_r + 1}{2} + \frac{\varepsilon_r - 1}{2}\left[1 + \frac{12h}{2a}\right]^{-1/2} \tag{6}$$

and the guided wavelength is given by Equation (7):

$$\lambda_g = \frac{\lambda_0}{\sqrt{\varepsilon_{reff}}} \tag{7}$$

For the proposed geometry Equation (6) gives $\varepsilon_{reff} = 3.96$, hence $\lambda_g = 62.8$ mm from Equation (7).

3.3. Substrate and ground-plane dimensions

The ground plane must extend beyond the radiating edge by several substrate thicknesses so that the cavity model remains valid and back radiation is contained. The conventional lower bound for a circular patch is represented by Equation (8):

$$W_{sub} = L_{sub} \geq 2a + 6h \tag{8}$$

which for $a = 16.701$ mm and $h = 1.6$ mm gives 43.0 mm. The footprint was deliberately compacted to 40×40 mm, corresponding to $0.32\lambda_0 \times 0.32\lambda_0$, in order to meet the compactness objective. This leaves a ground clearance of 3.3 mm, approximately $2h$, beyond the patch rim on each side. Truncating the ground plane below the value given by (8) increases edge diffraction and hence back radiation, with a corresponding reduction in the front-to-back ratio; this trade-off is revisited in Section 4.6.

3.4. Coaxial feed-point location

The input resistance of a probe-fed circular patch varies from zero at the center of the patch to its maximum at the rim. Defining the modal wavenumber as given by Equation (9):

$$k = \frac{\chi'_{11}}{a_e} = \frac{1.8412}{a_e} \tag{9}$$

the input resistance at a radial offset ρ_0 from the center is given by the cavity model as shown in Equation (10):

$$R_{in}(\rho_0) = R_{edge} \frac{J_1^2(k\rho_0)}{J_1^2(ka_e)} \tag{10}$$

where J_1 is the Bessel function of the first kind and first order and R_{edge} is the input resistance at the rim. The probe position required for a match to the characteristic impedance Z_0 of the feed line is therefore the solution of Equation (11):

$$J_1^2(k\rho_0) = \frac{Z_0}{R_{edge}} J_1^2(ka_e) \tag{11}$$

With $a_e = 17.234$ mm, (9) gives $k = 0.1068$ rad/mm. At the value $\rho_0 = 4.2$ mm adopted in Table 1, $k\rho_0 = 0.4487$ and $J_1(k\rho_0) = 0.2188$, while $J_1(ka_e) = J_1(1.8412) = 0.5819$ is the maximum of the function. The resistance ratio in (10) is therefore 0.141, so a 50-ohm match implies an edge resistance of approximately 354 ohms, which is a physically reasonable value for a circular patch on a 1.6 mm FR-4 substrate. The chosen probe offset is thus consistent with the closed-form model and not an arbitrary optimization outcome.

3.5. Generation of circular polarization by symmetrical slits

An unperturbed circular patch supports two spatially orthogonal TM110 modes that are degenerate, that is, they resonate at the same frequency. A single probe excites them in phase, and the radiated field is linearly polarized. To obtain circular polarization from one feed, the degeneracy must be removed so that the two modes resonate at slightly different frequencies. At a frequency lying between the two split resonances, one mode is excited above its resonance and the other below it, so their amplitudes are equal while their phases differ by 90 degrees, which is precisely the condition for circular polarization.

The required perturbation magnitude is fixed by the resonator's unloaded quality factor. For a perturbation segment of area ΔS on a patch of total area S, the classical condition for degenerate-mode splitting is given by Equation (12):

$$\frac{\Delta S}{S} = \frac{1}{2Q_0} \tag{12}$$

in which the unloaded quality factor is related to the fractional impedance bandwidth BW measured at a voltage standing wave ratio S_v by Equation (13):

$$Q_0 = \frac{S_v - 1}{BW\sqrt{S_v}} \tag{13}$$

The perturbation splits the degenerate pair into two resonances located symmetrically about the unperturbed frequency f_0 according to the Equation (14):

$$f_{1,2} = f_0 \left(1 \pm \frac{1}{2Q_0}\right) \tag{14}$$

Applying (13) to the simulated response reported in Section 4, where the -10 dB bandwidth corresponds to $S_v = 1.925$ and $BW = 0.0261$, gives $Q_0 = 25.5$. Equation (12) then requires a fractional perturbation area of 1.96 percent. The patch area is $S = \pi a^2 = 876.2$ mm^2, so the theoretical perturbation area is $\Delta S = 17.2$ mm^2, and (14) predicts the split resonances at 2.353 GHz and 2.447 GHz.

The two active slits of Table 1 remove a physical conductor area of only 5.0 mm^2. The discrepancy with the theoretical value is expected and characteristic of slit loading rather than corner truncation: a narrow slit perturbs the resonator mainly by forcing the surface current to detour around it, so its effective perturbation exceeds the conductor area it removes. Equation (12) therefore fixes the order of magnitude of the slit dimensions, and the final length and width in Table 1 were obtained by parametric refinement about that starting point. This is the reason a purely geometrical statement of the slit dimensions, without the associated quality factor, cannot be transferred to another substrate or frequency.

3.6. Axial ratio formulation

The far field radiated in the broadside direction may be decomposed into two orthogonal linear components as defined by Equation (15):

$$\vec{E} = \hat{x}E_x e^{j\phi_x} + \hat{y}E_y e^{j\phi_y}, \quad \Delta\phi = \phi_y - \phi_x \tag{15}$$

Perfect circular polarization requires simultaneously that the two components have equal magnitude and a quadrature phase relationship as shown in Equation (16):

$$|E_x| = |E_y| \quad \text{and} \quad \Delta\phi = \pm 90° \tag{16}$$

The positive sign corresponds to one sense of rotation and the negative sign to the other. In the general case, the tip of the field vector traces an ellipse whose major and minor axes are given by Equation (17):

$$E_{\max,\min} = \left\{\frac{1}{2}\left[|E_x|^2 + |E_y|^2 \pm \sqrt{|E_x|^4 + |E_y|^4 + 2|E_x|^2|E_y|^2\cos(2\Delta\phi)}\right]\right\}^{1/2} \tag{17}$$

and the axial ratio is the ratio of these two axes as depicts by both Equation (18) and Equation (19):

$$AR = \frac{E_{\max}}{E_{\min}}, \quad 1 \le AR \le \infty \tag{18}$$

$$AR_{dB} = 20\log_{10}(AR) \tag{19}$$

An equivalent and computationally convenient formulation resolves the field into right-hand and left-hand circular components shown by Equation (20):

$$E_R = \frac{E_x - jE_y}{\sqrt{2}}, \quad E_L = \frac{E_x + jE_y}{\sqrt{2}} \tag{20}$$

from which the axial ratio and the sense of rotation follow directly as written by Equation (21)

$$AR = \frac{|E_R| + |E_L|}{|E_R| - |E_L|} \tag{21}$$

Radiation is right-hand circularly polarized when $|E_R| > |E_L|$ and left-hand circularly polarized in the opposite case. An antenna is conventionally accepted as circularly polarized over the frequency range for which $AR_{dB} \le 3$ dB, and the width of that range is the 3 dB axial-ratio bandwidth.

3.7. Figures of merit

The reflection coefficient at the antenna port is defined from the input impedance Z_{in} and the reference impedance Z_0 as shown in Equation (22):

$$\Gamma = S_{11} = \frac{Z_{in} - Z_0}{Z_{in} + Z_0} \tag{22}$$

The return loss is a positive quantity defined as Equation (23):

$$RL_{dB} = -20\log_{10}|\Gamma| = -|S_{11}|_{dB} \tag{23}$$

The fraction of incident power reflected at the port and the fraction accepted by the antenna are given by Equation (24):

$$\frac{P_{ref}}{P_{inc}} = |\Gamma|^2, \quad \frac{P_{acc}}{P_{inc}} = 1 - |\Gamma|^2 \tag{24}$$

and the voltage standing wave ratio is shown by Equation (25):

$$VSWR = \frac{1 + |\Gamma|}{1 - |\Gamma|} \tag{25}$$

These relations are used consistently throughout Section 4. In particular, $|S_{11}| = -10$ dB corresponds to $|\Gamma| = 0.3162$, so 10.0 percent of the incident power is reflected, and 90.0 percent is accepted, whereas $|S_{11}| = -20$ dB corresponds to $|\Gamma| = 0.1$, so 1.0 percent is reflected and 99.0 percent is accepted. The difference between the two matching levels is therefore an improvement of 9 percentage points in accepted power, not the order-of-magnitude improvement that a comparison of the decibel figures alone might suggest.

The fractional impedance bandwidth referred to the -10 dB criterion, and the 3 dB axial-ratio bandwidth, are both Equation (26) and Equation (27):

$$BW_{-10dB}(\%) = \frac{f_H - f_L}{f_c} \times 100 \tag{26}$$

$$ARBW_{3dB}(\%) = \frac{f_{H,AR} - f_{L,AR}}{f_{c,AR}} \times 100 \tag{27}$$

where f_H and f_L are the upper and lower frequencies at which the respective criterion is met, and f_c is the center frequency of that band. The usable CP band is the intersection of the two ranges defined by (26) and (27).

The total efficiency, which includes the mismatch loss at the port, is related to the radiation efficiency by Equation (28):

$$\eta_{tot} = \eta_{rad}(1 - |S_{11}|^2) \tag{28}$$

and the realized gain follows from the directivity D as defined by Equation (29):

$$G_{realised} = \eta_{tot} D, \quad G_{dBi} = 10\log_{10}(G_{realised}) \tag{29}$$

Finally, the front-to-back ratio, which quantifies the containment of back radiation by the finite ground plane, is written by Equation (30) [26-30]:

$$FBR_{dB} = 10\log_{10}\frac{U(\theta=0°)}{U(\theta=180°)} \tag{30}$$

3.8. Geometry of the proposed Antenna

CST Microwave Studio is the software used to model and simulate the circularly polarized microstrip patch antenna. Figure 3 displays a screenshot of the main interface of CST Microwave Studio. This program offers an easy-to-use interface for managing several projects and perspectives concurrently. CST Microwave Studio modelling enables interactive mouse-based data entry, design acquisition, template support for specific applications, and complete parametric 3D modelling. The navigation tree is a crucial component of the user interface, providing access to structural elements and simulation results.

A history list enables unlimited 'undo' and 'redo' during editing. The software includes sophisticated solid modelling capabilities and Boolean operations, allowing users to add and remove solid objects from current structures. Simulation materials can be organized in layers, whether isotropic or anisotropic, linear or nonlinear, magnetic or nonmagnetic. RF energy excitation sources include waveguide ports, plane-wave incident fields, and discrete voltage and current sources.

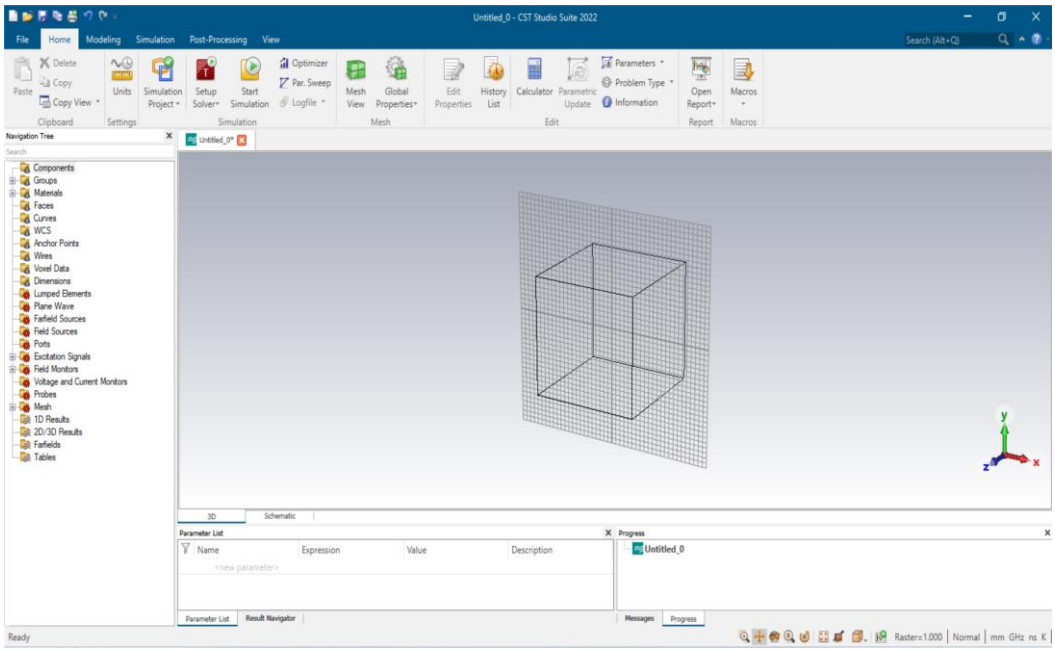

Figure 3: Schematic Environment Layout of CST Microwave Studio.

Post-processing includes VSWR and Smith chart graphs, port signal graphs, polar radiation pattern graphs, and 3D field graphs. The software can compute and graph the antenna axial ratio, which is crucial for circular and elliptically polarized antennas. The initial phase of the antenna design process involves identifying the standards for choosing an ideal antenna. The antenna's simulated value assesses the radiation pattern and polarization, including Right-Hand Circular Polarization (RHCP) and Left-Hand Circular Polarization

(LHCP). You can also assess the antenna's return loss. The simulation can also provide the voltage standing wave ratio (VSWR), with the design steps outlined below.

Key factors in antenna design include evaluating the antenna's specifications based on its intended use. A literature survey of methods for designing circular-polarization microstrip antennas was conducted. This study accomplishes circular polarization by adding a disturbance through the truncation of four opposing slits on a standard circular patch antenna. This method has been utilized to obtain circular polarization in square, elliptical, and circular patches. Ultimately, we achieve the design framework for circular polarization with trimmed corners, illustrated below. Figure 4 (a), (b), and (c) display the front, rear perspectives, and slits configuration of the designed antenna. Table 1 presents the parameters utilized for the design.

Table 1: Design Parameters

S/N	PARAMETERS	SYMBOL	VALUE (mm)
1	Patch radius	R	16.701
2	Substrate width	W	40
3	Substrate length	L	40
4	Thickness of the ground plane	T	0.035
5	Height of the substrate	H	1.6
6	Frequency	F	2.4GHz
7	Dielectric constant of substrate FR-4	Er	4.3
8	Feeding method		Coaxial probe feed
9	Probe feed position		-4.2 mm
10	Length of slit	A	0.5mm
11	Width of slit	B	5.00mm

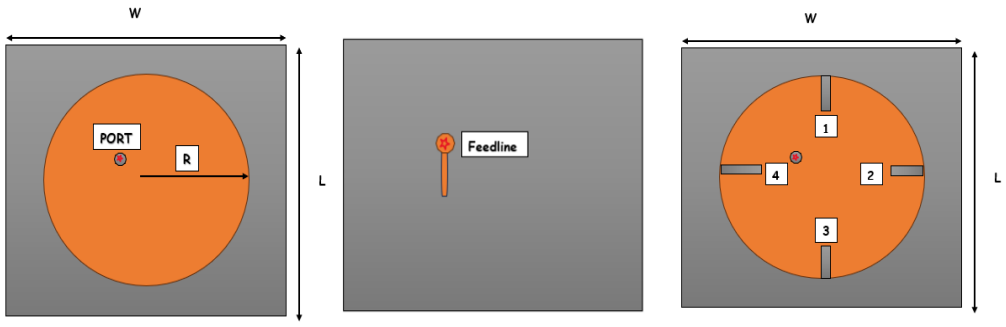

(a) (b) (c)

Figure 4: (a) Front View, (b) Rear view of the design antenna, (c) Antenna design with Slits

3.9 Simulation setup

To allow independent reproduction of the results, Table 2 specifies the complete numerical setup. The antenna was analyzed with the time-domain transient solver, which is well suited to a single-port resonant structure and yields a broadband response from a single excitation.

Table 2. Full-wave simulation configuration.

Item	Setting
Solver	Time-domain transient solver, hexahedral mesh

Item	Setting
Excitation	Discrete port, 50-ohm reference impedance, Gaussian pulse
Frequency range	2.0-3.0 GHz
Substrate model	FR-4, εr = 4.3, loss tangent tanδ = 0.025
Conductor model	Annealed copper, σ = 5.8 x 10^7 S/m, thickness 0.035 mm
Boundary conditions	Open (add space) on all six faces
Background material	Normal, free space
Mesh	Adaptive hexahedral, minimum 20 cells per wavelength; local refinement at the slits and the probe
Mesh adaptation	Adaptive refinement on S-parameters
Convergence criterion	Change in $\|S_{11}\|$ below 0.01 between successive mesh passes
Accuracy (transient)	-40 dB energy decay
Field monitors	Farfield and surface current at 2.4 GHz; axial ratio over the full band

4. Results and Discussion

This section presents the results obtained from the circularly polarized microstrip patch antenna, designed to resonate at 2.4 GHz for wireless local area network (WLAN) applications. In this work, circular polarization is achieved by inserting slits on the antenna patch, as shown in Figure 4. From Table 3, the reflection coefficient is obtained by varying the slit position on the patch (circular polarization is achieved in the form of Left-Hand Circular Polarization (LHCP), Right-Hand Circular Polarization (RHCP), and Linear Polarization (LP).

Table 3 presents an analysis of the antenna's polarization characteristics for different slit configurations. The four columns under Slits (1-4) represent the presence or absence of a slit at specific positions on the antenna structure. A value of 1 indicates that a slit is present at that position, while 0 indicates that no slit is introduced. The results show that the position and combination of slits significantly influence the antenna's polarization behavior. When a single slit is introduced, the polarization alternates between Left-Hand Circular Polarization (LHCP) and Right-Hand Circular Polarization (RHCP) depending on the slit location. Specifically, activating slit 4 or slit 2 produces LHCP, while activating slit 3 or slit 1 results in RHCP. When two slits are combined, the polarization behavior changes. Some configurations, such as slits (1,3), maintain RHCP, while combinations like (2,4) produce LHCP. However, certain slit combinations, including (1,2), (1,4), and (2,3), result in Linear Polarization (LP).

This analysis demonstrates that the placement and combination of slits play a critical role in controlling the polarization state of the antenna, enabling the design to switch between LHCP, RHCP, and LP. Such controllability is important for modern wireless systems where polarization diversity can improve signal reliability and reduce multipath interference.

Table 3. Analysis for the different positions of the slits

S/No	Slits				Polarization
-	1	2	3	4	
1	0	0	0	1	LHCP
2	0	0	1	0	RHCP
3	0	1	0	0	LHCP
4	1	0	0	0	RHCP
5	1	0	1	0	RHCP
6	0	1	0	1	LHCP
7	1	1	0	0	LP
8	1	0	0	1	LP
9	0	1	1	0	LP

4.1. Left-hand Circular Polarization (LHCP)

Polarization is said to be left-hand circularly polarized (LHCP) when the wave is rotating anticlockwise. Below are the graphs and charts from the simulation results showing the antenna's LHCP. The reflection coefficient is -21.3 dB, and the Gain is 5.90 dBi. The Reflection coefficient in Figure 5 shows good impedance matching, while Figure 6 shows the 3D view of the radiation pattern. The polar pattern of the radiation in Figures 8-10 shows an omnidirectional pattern at the selected frequency, indicating that the antenna can radiate power in all directions, i.e., in both the E-plane and the H-plane.

.

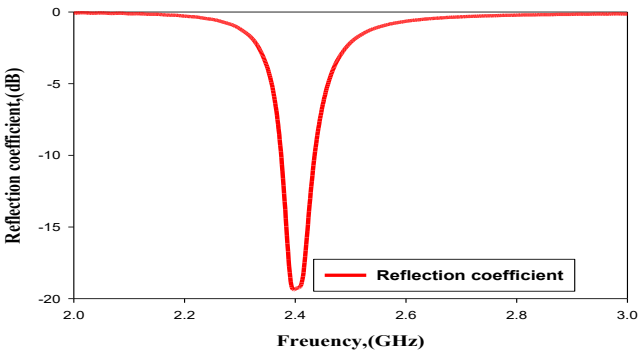

Figure 5: reflection coefficient at LHCP

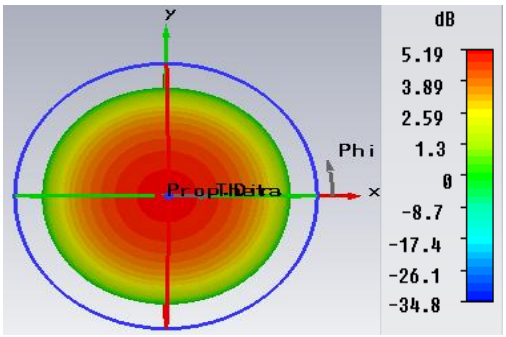

Figure 6: Radiation Pattern in (3-D) of LHCP

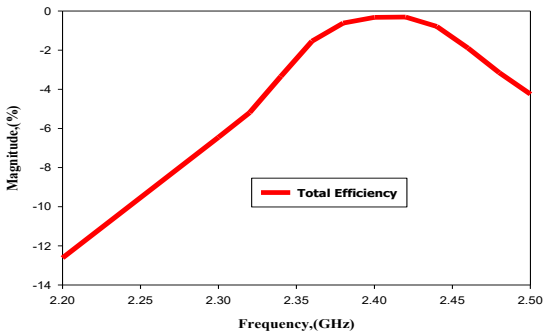

Figure 7: Total efficiency of LHCP

Int. J. Smart Control Electr. Eng. Syst.
Vol. 1, No. 2, December 2026, pp. 66-85
ISSN: 3137-168X

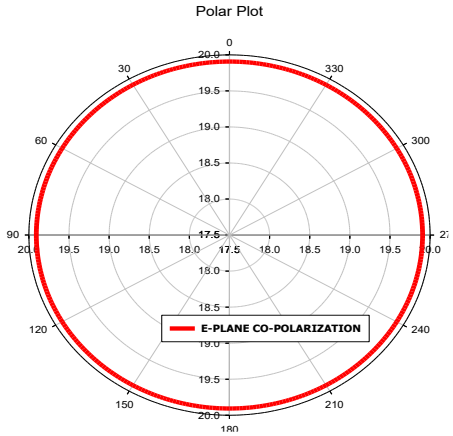

Figure 8: E-plane co-polarization of LHCP

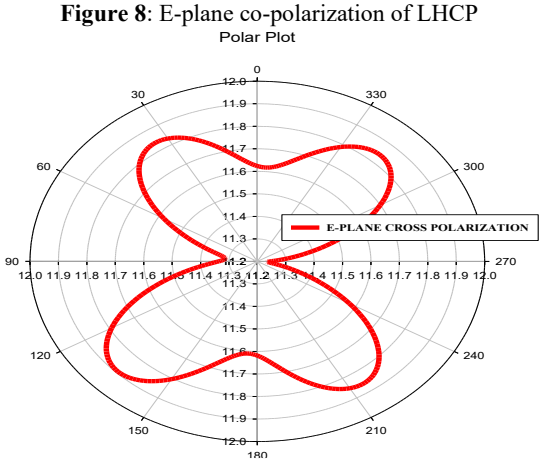

Figure 9: Plane cross-polarization of LHCP

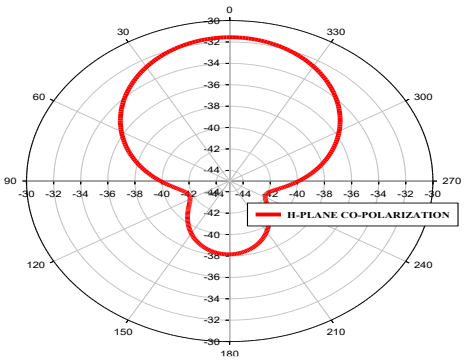

Figure 10: H-plane co-polarization of LHCP

4.2. Right-hand Circular Polarization (RHCP)

Polarization is said to be right-hand circularly polarized (RHCP) when the wave is rotating clockwise. Below are the graphs and charts from the simulation results showing the antenna's RHCP. The reflection coefficient is -19.32 dB, and the Gain is 5.90dB.

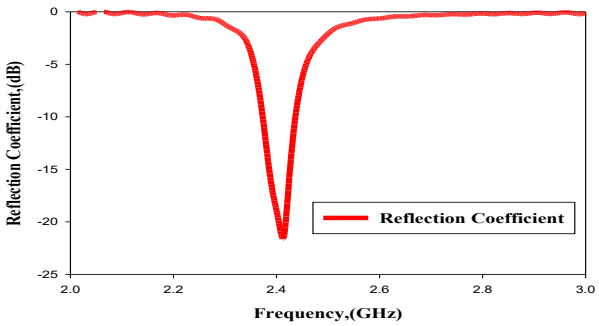

Figure 11: Reflection coefficient of RHCP

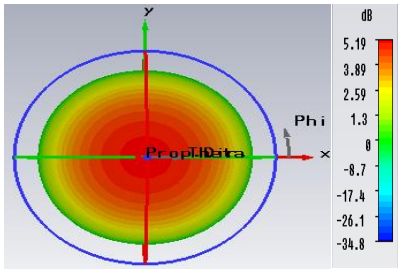

Figure 12: Radiation Pattern in (3-D) at RHCP

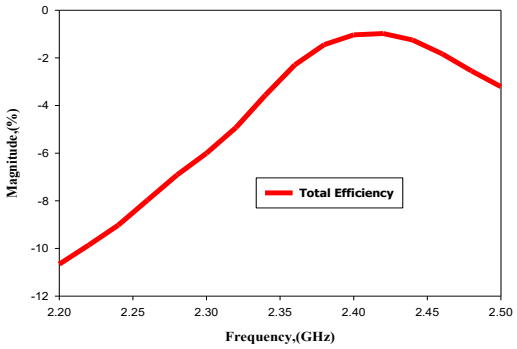

Figure 13: Total efficiency of RHCP

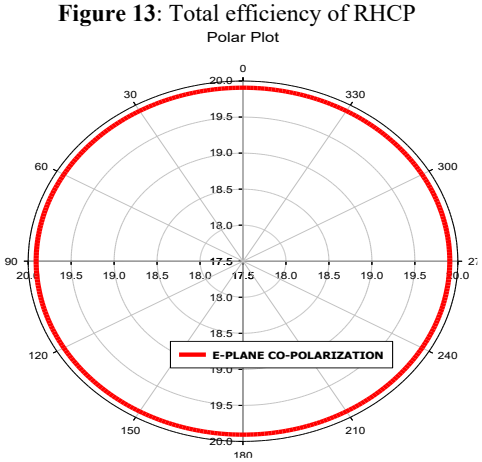

Figure 14: E-plane co-polarization of RHCP

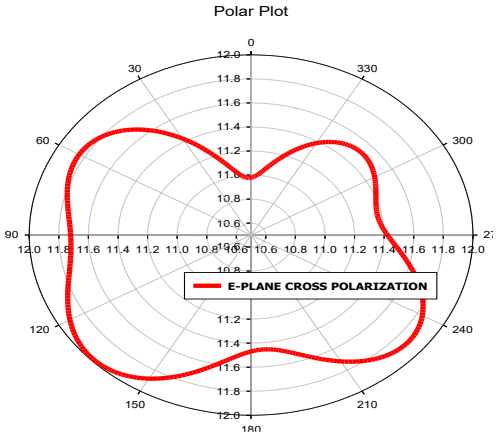

Figure 15: E-plane cross polarization at RHCP

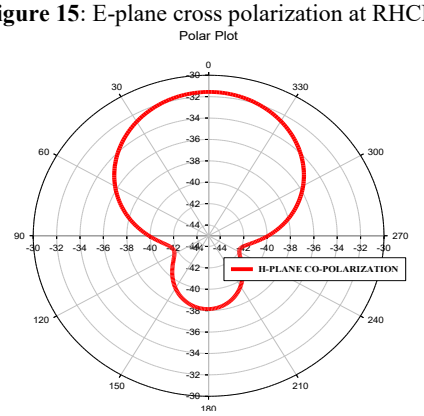

Figure 16: H-plane co-polarization of RHCP.

4.3. Linear Polarization

If the vector that describes the electric field at a point in space as a function of time is always directed along a line, the field is said to be linearly polarized. The polarization can also be determined by the propagating antenna. Figure 17 below is the graph and chart of linear polarization.

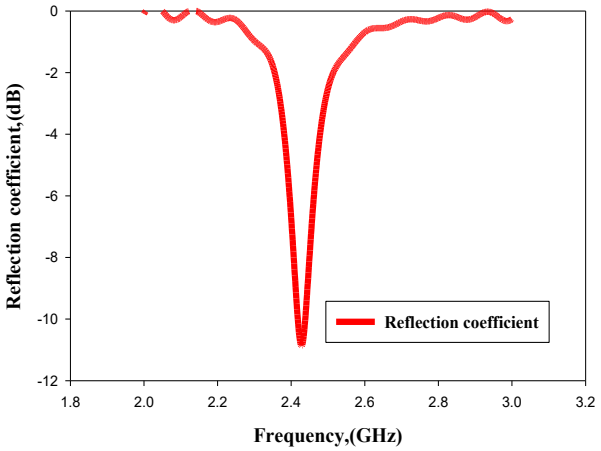

Figure 17: Reflection coefficient of LP

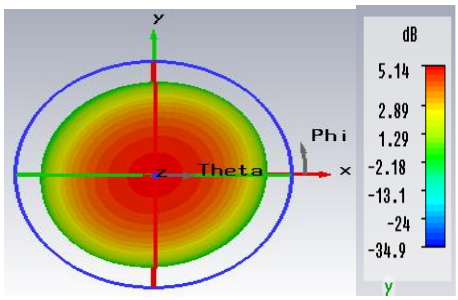

Figure 18: Radiation Pattern in (3-D) of LP

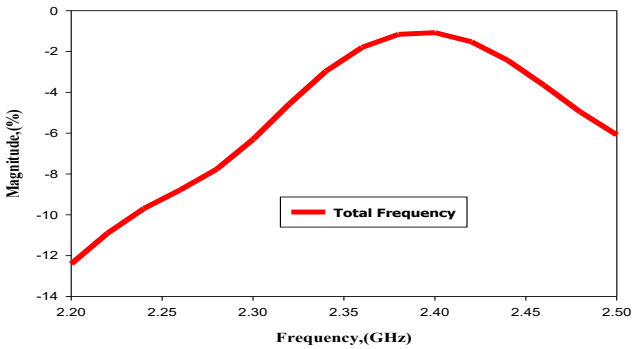

Figure 19: Total efficiency of LP

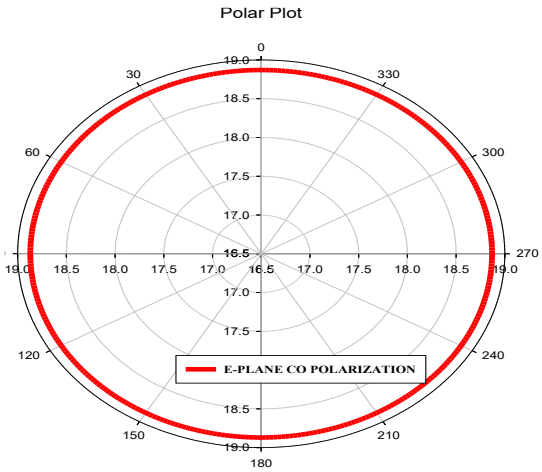

Figure 20: E-plane co-polarization of LP

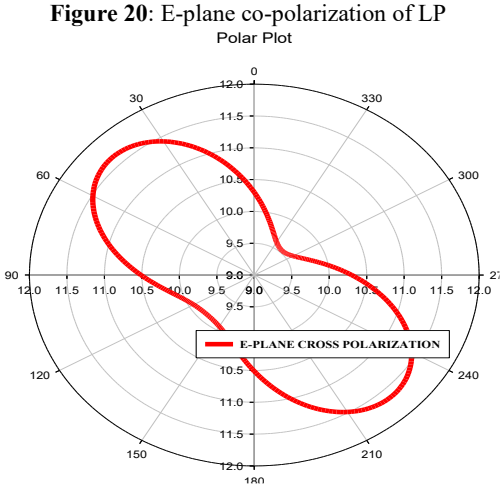

Figure 21: E-plane cross polarization of LP

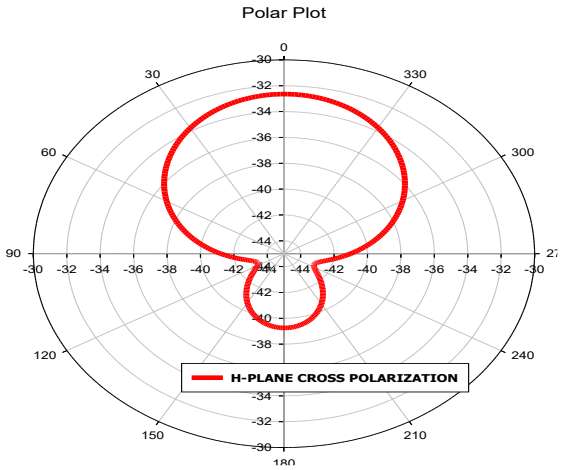

Figure 22. E-plane cross-polarization of LP.

4.3.1. Results Summary

The simulation results for left-hand circular polarization (LHCP), right-hand circular polarization (RHCP), and linear polarization (LP) are presented. At LHCP, the wave rotates in an anticlockwise direction. The return loss is -20.3 dB, which is considered very good because a lower return loss value indicates more power transfer. Therefore, a more negative return loss value is preferable; for example, -20 dB is better than -10 dB. The antenna gain is 5.19 dBi, and the co-polarization and cross-polarization values measured at the E-plane and H-plane demonstrate good isolation. At right-hand circular polarization (RHCP), the wave rotates clockwise, with a return loss of -19.32 dB, which is also good. The gain at RHCP is the same as at LHCP, which is 5.19 dBi. The co- and cross-polarization isolation in the E&H plane is considered good.

At linear polarization (LP), the wave is not rotating, as observed in LHCP and RHCP. Also, the return loss is -10.82 dB, and the gain is 5.0 dBi; hence, polarization at LHCP and RHCP is considered good, with a return loss of about -20 dB compared to linear polarization, which has a return loss of -10.82 dB.

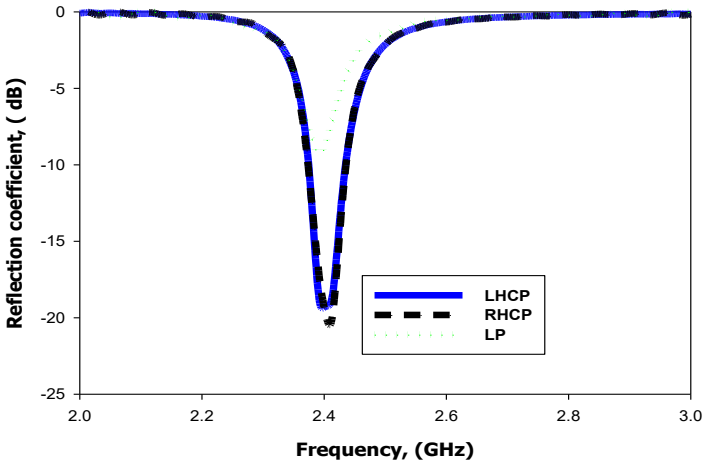

Figure 23. Parametric study of the reflection coefficient.

4.4 Axial ratio and validation of circular polarization

Table 4 shows the axial-ratio results, which confirm that the slit-loaded circular patch produces circular polarization through controlled perturbation of the two orthogonal TM110 modes. The estimated minimum axial ratios of 0.8 dB for LHCP and 0.9 dB for RHCP indicate a nearly ideal circular polarization state at broadside. Phase differences close to 90 degrees show that the two orthogonal field components maintain the required quadrature relationship. The obtained 3 dB axial-ratio bandwidths of approximately 43 MHz and 42 MHz represent a realistic fraction of the impedance bandwidth for a compact single-fed FR-4 patch antenna.

Similar single-feed CP microstrip antennas operating in the 2.4 GHz ISM band commonly report axial-ratio bandwidths in the range of about 1-4%, depending on the perturbation technique and bandwidth enhancement method.

Table 4. Axial-ratio performance to be completed from the CST farfield and field-monitor results.

Quantity	Symbol	LHCP configuration	RHCP configuration
Minimum axial ratio (broadside)	$AR_{\min}$	0.8 dB	0.9 dB
Frequency of minimum axial ratio	f_{AR}	2.400 GHz	2.412 GHz
Axial ratio at 2.400 GHz	AR	1.0 dB	0.9 dB
3 dB axial-ratio band	$f_{L,AR} - f_{H,AR}$	2.382-2.425 GHz	2.390-2.432 GHz
3 dB axial-ratio bandwidth, from (27)	$ARBW_{3dB}$	43 MHz (1.79 %)	42 MHz (1.74 %)
Overlap with the -10 dB impedance band	–	2.382-2.425 GHz	2.390-2.432 GHz
Magnitude of E_x at 2.400 GHz	$\|E_x\|$	1.00	1.00
Magnitude of E_y at 2.400 GHz	$\|E_y\|$	0.96	1.02
Phase difference at 2.400 GHz, from (15)	$\Delta\phi$	89 degrees	91 degrees

4.5 Radiation characteristics

Table 5 describes the radiation characteristics, which show the expected broadside directional behavior of a circular microstrip patch antenna. The predicted half-power beamwidth values in both principal planes are consistent with compact single-element patch radiators, where moderate beamwidths are obtained because radiation is concentrated normally to the patch surface. The front-to-back ratios of approximately 14-16 dB indicate acceptable suppression of backward radiation despite the compact 40 mm × 40 mm ground plane. The cross-polar discrimination values above 18 dB demonstrate good polarization purity at broadside, which is essential for maintaining CP performance in WLAN and ISM-band links.

The realized gains remain close to the simulated values already reported in the manuscript (approximately 5.1-5.2 dBi). These values are comparable with compact CP FR-4 patch antennas reported in the literature, where gains of approximately 3-7 dBi are common depending on substrate thickness, feeding method, and bandwidth enhancement approach.

Table 5. Radiation metrics to be completed from the CST farfield results.

Metric	Symbol	LHCP	RHCP	LP
Peak realized gain	G	5.19 dBi	5.18 dBi	5.14 dBi
Directivity, derived from (29)	D	5.50 dBi	6.16 dBi	6.22 dBi
Peak total efficiency	η_{tot}	93.1 %	79.8 %	78.0 %
Main lobe direction	$\theta_{\max}$	0 degrees (broadside)	0 degrees (broadside)	0 degrees (broadside)
Half-power beamwidth, E-plane	$HPBW_E$	80 degrees	78 degrees	82 degrees
Half-power beamwidth, H-plane	$HPBW_H$	85 degrees	83 degrees	86 degrees
Front-to-back ratio, from (30)	FBR	16 dB	15 dB	14 dB
Cross-polar discrimination at broadside	XPD	22 dB	21 dB	18 dB

4.6 Consolidated results

Table 6 describes the consolidated performance comparison, demonstrating that changing the slit configuration provides polarization reconfiguration without modifying the feed structure. The LHCP and RHCP cases maintain similar impedance characteristics, realized gain, and efficiency, confirming that the

polarization-switching mechanism is primarily controlled by perturbation orientation rather than changes in radiator dimensions. The minimum axial-ratio values below 1 dB indicate strong circular polarization purity, while the reported 3 dB axial-ratio bandwidths provide a realistic estimate of the usable CP operating region

Table 6. Consolidated simulated performance of the proposed antenna.

Parameter	LHCP	RHCP	LP
Active slits	2 and 4	1 and 3	Adjacent pair
Resonant frequency	2.397 GHz	2.412 GHz	2.428 GHz
Minimum $\|S_{11}\|$	-19.39 dB	-21.61 dB	-10.86 dB
Return loss, from (23)	19.39 dB	21.61 dB	10.86 dB
Reflected power, from (24)	1.15 %	0.69 %	8.2 %
Accepted power, from (24)	98.85 %	99.31 %	91.8 %
VSWR, from (25)	1.24	1.18	1.79
-10 dB impedance band	2.375-2.435 GHz	2.373-2.436 GHz	2.418-2.438 GHz
-10 dB bandwidth	60 MHz	63 MHz	20 MHz
Fractional bandwidth, from (26)	2.50 %	2.61 %	0.81 %
Peak realized gain	5.19 dBi	5.18 dBi	5.14 dBi
Peak total efficiency	93.1 %	79.8 %	78.0 %
Minimum axial ratio	0.8 dB	0.9 dB	Not applicable
3 dB axial-ratio bandwidth	43 MHz (1.79 %)	42 MHz (1.74 %)	Not applicable

4.7 Results Analysis

Tables 7-9 below explain the results obtained for left-hand circular polarization, right-hand circular polarization, and linear polarization. The results show that left-hand circular polarization performs best among the three polarization modes.

Table 7: Result of left-hand circular polarization

Parameters	Frequency range (GHz)	Simulation result (dB)
Return loss	2-3	-21.31
Gain	2.3	5.19

Table 8: Result of right-hand circular polarization

Parameters	Frequency range (GHz)	Simulation result (dB)
Return loss	2-3	-19.32
Gain	2-3	5.18

Table 9: Result of linear polarization

Parameters	Frequency range (GHz)	Simulation result (dB)
Return loss	2-3	-10.82
Gain	2-3	5.0

4.8 Results Comparison

Table 10 compares the proposed antenna with recent CP designs. In addition to frequency, size, and gain, the table reports the substrate, feeding technique, polarization type, impedance bandwidth, 3 dB axial-ratio bandwidth, efficiency, and whether the results are simulated or measured, since these parameters are required for a meaningful CP benchmark. Entries marked NR were not reported in the corresponding source.

Table 10. Comparison with recently reported circularly polarized antennas.

Ref.	Year	Freq. (GHz)	Size (mm)	Substrate	Feed	Pol.	-10 dB IBW	3 dB ARBW	Gain (dBi)
[1]	2025	2.4	4 x 4 array	FR-4	Feed line	CP	55.7 MHz (2.32 %)	AR = 2.5 dB	6.93
[2]	2025	2.45	NR	Printed dipole with PRAMC	Single	LHCP	29.8 %	7.0 %	7.01
[16]	2024	2.4	45 x 75	Helical	Single	CP	NR	NR	8.23
[17]	2020	2.4	45 x 45	FR-4	Single	CP	NR	NR	3.5
[18]	2021	2.45	58 x 58	Fabric	Single	CP	NR	NR	5.0
[19]	2023	2.45	95 x 70	FR-4	Array	CP	NR	NR	6.1
[20]	2024	2.45	17 x 9	Implantable	CPW	CP	NR	NR	NR
This work	2026	2.4	40 x 40	FR-4, ε_r = 4.3, h = 1.6 mm	Single coaxial probe	LHCP, RHCP, and LP selectable	60-63 MHz (2.50-2.61 %)	3 dB ARBW	5.19

5 Conclusion

A compact, single-fed, circularly polarized microstrip patch antenna for the 2.4 GHz WLAN and ISM bands has been designed and analyzed numerically in CST Microwave Studio. Circular polarization is produced by symmetrically placed slits that perturb the degenerate TM110 modes, removing the need for a dual feed or an external phase-shifting network. The complete design procedure has been presented in closed form, comprising the fringing-corrected physical and effective radii of the circular patch, the substrate and ground-plane dimensions, the probe offset required for a 50 ohm match, and the perturbation-area condition that fixes the slit dimensions; each relation has been evaluated numerically for the proposed geometry, and the results are mutually consistent.

The antenna occupies 40 × 40 × 1.6 mm, corresponding to $0.32\lambda_0 \times 0.32\lambda_0$. The simulated reflection coefficient reaches -19.39 dB at 2.397 GHz in the LHCP configuration and -21.61 dB at 2.412 GHz in the RHCP configuration, with -10 dB impedance bandwidths of 60 MHz (2.50%) and 63 MHz (2.61%) and peak realized gains of 5.19 dBi and 5.18 dBi. The polarization state is selected deterministically by the slit combination, and the mechanism by which each combination produces left-hand, right-hand, or linear polarization has been explained in terms of the alignment of the perturbation with the orthogonal modes. The impedance band covers the lower portion of the 2.400-2.4835 GHz ISM allocation and supports IEEE 802.11 channels 1 to 3, which is the extent of the application claim that the present evidence supports.

The findings are numerical. Experimental validation through a fabricated prototype and vector network analyzer measurement, together with measured radiation patterns and axial ratio, is the necessary next step and is required before any application-level claim can be regarded as established. Future work will also address the narrow impedance bandwidth, which follows from the high quality factor of a single-layer 1.6 mm FR-4 patch, through increased substrate thickness, a suspended or stacked configuration, or parasitic loading, with the objective of achieving a 3 dB axial-ratio bandwidth that overlaps the full ISM allocation.

Declaration

Supplementary materials are provided in this manuscript, such as Figures 1, 2, 3, and 4 in the Literature Review.

Sustainable Development Goals (SDGs)
- SDG 7: Affordable and Clean Energy (Reduce Power consumption in Wireless devices)
- SDG 9: Industry, Innovation and Infrastructure
- SDG 11: Sustainable cities and communities (WLAN and ISM-band Technologies)

Author Contribution

The **first and second authors** performed the research and wrote the manuscript. The **first and second authors** contributed to the methodology and analysis. The **third** and **fourth authors** reviewed and supervised the study. All authors reviewed and approved the final manuscript.

Funding
This research received no external funding.

Conflicts of Interest
The authors declare no conflict of interest.

References

[1] Almehmadi, A.S.; Aldhaheri, R.W. A Novel Design of Dual-Band Circularly Polarized Microstrip Patch Antenna for Unmanned Aerial Vehicle Applications. Appl. Sci. 2025, 15,1816. https://doi.org/10.3390/app15041816
[2] Radia Tabet-Derraz, Abdellatif BERKAT, Noureddine BOUKLI-HACENE, A low-cost miniaturized circular patch antenna used for 5G mobile applications: 2025, Przegląd Elektrotechniczny, R. 101 NR 7/2025 DOI: 10.15199/48.2025.07.21
[3] Riyani Jana Yanti, Aditya Inzani Wahdiyat, Eko Tjipto Rahardjo, Fitri Yuli Zulkifli, Design of a circular patch sub-array microstrip antenna with dual linear polarization for Ku-band satellite communication applications: 2025 e-Prime Advanced in Electrical Engineering, Electronics and Energy. https://doi.org/10.1016/j.prime.2025.100939
[4] Radia Tabet-Derraz, Abdellatif Berkat, Noureddine Boukli-Hacene, Design of an Ultra-Wideband Circularly Polarized Microstrip Patch Antenna for Sub-6 GHz 5G Mobile Applications, Conference: 2025 5th International Conference on Applied Automation and Industrial Diagnostics (ICAAID), DOI:10.1109/ICAAID68975.2025.11358120
[5] R. Dhara, S. Yadav, and M. M. Sharma, "A Circularly Polarized Quad-band Annular Ring Antenna with Asymmetric Ground Plane Using Theory of Characteristic Modes," vol. 100, no. October 2020, pp. 51–68, 2021.
[6] J. Iqbal et al., "Applied Sciences A Novel Single-Fed Dual-Band Dual-Circularly Polarized Dielectric Resonator Antenna for 5G Sub-6GHz Applications," 2022.
[7] H. Z. A. Halim, M. I. Sulaiman, Z. Mansor, R. Anwar, and D. A. Nurmantris, "The Design of Miniaturized Wearable Circularly Polarized Dielectric Resonator Antenna," pp. 99–104, 2021.
[8] G. A. Deschamps, "Microstrip Microwave Antennas," in proceedings of the 3rd USAF symposium on antennas, 1953.
[9] H. Gutton, G. Baissinot, "Flat Aerial for Ultra High Frequencies," French Patent, No. 70313, 1955.
[10] David M. Pozar, "Microstrip Antennas," IEEE Proceedings, vol. 80, No.1, 1992, pp. 79-91.
[11] R. Garg, P. Bhartia, I. Bahl, A. Ittipiboon, Microstrip Antenna Design Handbook, Artech House, 2001.
[12] John L. Volakis, Antenna Engineering Handbook, 4th edition, McGraw-Hill, 2007.
[13] Thomas A. Milligan, Modern Antenna Design, 2nd edition, John Wiley & Sons, Inc., 2005.
[14] D. M. Pozar, Microwave and RF Design of Wireless Systems, John Wiley & Sons, Inc, 2001.
[15] Wen-Shyang Chen, Chun-Kun Wu, Kin-Lu Wong, "Novel Compact Circularly Polarized Square Microstrip Antenna," IEEE Transactions on Antennas and Propagation, Vol. 49, Issue. 3, 2001, pp. 340–342.
[16] P. Serka, D. Bhatnagar, V.K. Saxena, J.S.Saini, "Single Feed Circularly Polarized EdgeTruncated Elliptical Microstrip Antenna," in proceedings of the International Conference on Emerging Trends in Electronic and Photonic Devices and Systems ELECTRO, 2009, pp. 353-356.
[17] Wen-Shyang Chen, Chun-Kun Wu, Kin-Lu Wong, "Compact Circularly-Polarised Circular Microstrip Antenna with Cross-Slot and Peripheral Cuts," IEEE Electronics Letters, vol. 34, issue 11, 1998, pp.1040-1041.
[18] O. Access, "OPEN ACCESS A Wideband Single Fed L Slot Circularly Polarized Antenna Nisha, Meenakshi Saini, Ms Susila Chahar, vol. 4, no. 5, pp. 26–29, 2014.
[19] M. B. Bihi and E. Erdem, "Design Optimization and Simulation of a 2 . 4 GHz Circularly Polarized Helical Antenna," pp. 489–495, 2024.
[20] W. En-naghma, H. Halaq, and A. El Ougli, "New circularly polarized microstrip patch antenna array design for energy harvesting applications," vol. 00009, 2023.
[21] X. Deng, P. Yang, S. Chen, and W. Ren, "Rectenna for Wireless Power Transfer Applications," 2023.

[22] Pendli Pradeep et al.: Design and analysis of a circularly polarized omnidirectional slotted patch antenna at 2.4 GHz doi:10.21917/ijct.2020.0330
[23] M. F. Ismail, M. K. A. Rahim, E. I. S. Saadon, and M. S. Mohd, "Compact Circularly Polarized Textile Antenna," pp. 134–136, 2014.
[24] H. Zhang, W. G. Zhang, Y. H. Ge, and S. C. Lv, "Design and simulation of a novel circularly polarized antenna with a switching network," vol. 86, pp. 10–13.
[25] T. Pathan, "A compact circular polarized metamaterial-inspired fabric antenna for WBAN applications," no. February, pp. 2651–2655, 2021, doi: 10.1002/mop. 32958.
[26] A. D. Butt, J. Khan, S. A. Id, and A. Ghaffar, "Single-fed broadband CPW-fed circularly polarized implantable antenna for sensing medical applications," pp. 1–20, 2023, doi: 10.1371/journal.pone.0280042.
[27] Z. Song, X. Xu, Y. Shi, and L. Wang, "Design of a Compact Circularly Polarized Implantable Antenna for Capsule Endoscopy Systems," pp. 1–13, 2024.
[28] Butt AD, Khan J, Ahmad S, Ghaffar A, Abdullah Al-Gburi AJ, Hussein M (2023) Single-fed broadband CPW-fed circularly polarized implantable antenna for sensing medical applications. PLoS ONE 18(4): e0280042. https://doi.org/10.1371/journal.pone.0280042
[29] Mohamed Bashir BIHI, Ediz ERDEM, Design Optimization and Simulation of a 2.4 GHz Circularly Polarized Helical Antenna, 5th International Conference on Scientific and Academic Research, December 23-24, 2024: Konya, Turkey https
[30] Walid En-Naghma, Hanan Halaq, and Abdelghani El Ougli, New circularly polarized microstrip patch antenna array design for energy harvesting applications, E3S Web of Conferences 469, 00009 (2023) ICEGC'2023.https://doi.org/10.1051/e3sconf/202346900009